# The Shape of a Stretched Polymer

Alberto S. Sassi, Salvatore Assenza, and Paolo De Los Rios

*Laboratoire de Biophysique Statistique, Ecole Polytechnique Fédérale de Lausanne (EPFL), CH-1015 Lausanne, Switzerland*

The shape of a polymer plays an important role in determining its interactions with other molecules and with the environment, and is in turn affected by both of them. As a consequence, in the literature the shape properties of a chain in many different conditions have been investigated. Here, we characterize the shape and orientational properties of a polymer chain under tension, a physical condition typically realized both in single-molecule experiments and *in vivo*. By means of analytical calculations and Monte Carlo simulations, we develop a theoretical framework which quantitatively describes these properties, highlighting the interplay between external force and chain size in determining the spatial distribution of a stretched chain.

Polymer chains are strongly-fluctuating objects. Due to their soft nature, they do not have well-defined shapes, but rather adapt their conformational ensembles to the environment surrounding them. At the same time, the shape of a polymer affects the way it interacts with other molecules in solution, *e.g.* quantitatively determining the excluded volume of the chain, thus ultimately influencing the thermodynamic properties of the solution [1, 2]. In a poor solvent, polymers collapse into a roughly spherical shape, as seen for example in the case of single-chain globular proteins [3]. In the case of $\theta$- or good-solvent conditions, conformations can fluctuate more wildly and the shape of a polymer is more sensitive to the environment. In the last two decades, many theoretical and experimental works have investigated how the shape depends on several factors such as confinement [4–6], topology [7–9] or crowding [3, 10–12], which are relevant to many cellular processes.

*In vivo* biopolymers are often under the action of mechanical forces. For example, during replication DNA is repeatedly pulled and twisted by enzymes [13], and proteins are actively pulled by chaperones across membranes and out of ribosomes [14–19]. Moreover, the recent development of several single-molecule techniques such as AFM, Optical and Magnetic Tweezers has stimulated a large amount of experimental works involving polymer stretching [20]. Surprisingly, in spite of the great importance of stretched chains for both *in vivo* and single-molecule studies, a proper account for the effect of an external pulling force on the shape of a polymer has been lacking, even at the simplest level. Here we compute, by means of both analytical calculations and Monte Carlo (MC) simulations, some key global quantities characterizing the shape of a stretched chain. Particularly, we focus on the simple case of the Freely Jointed Chain (FJC) model, a useful representation of a polymer in a good solvent where the conformation of a chain made by $N+1$ monomers is described as a three-dimensional Random Walk $\{\boldsymbol{R}_i\}_{i=0}^{N}$, where the segments $\boldsymbol{r}_i \equiv \boldsymbol{R}_i - \boldsymbol{R}_{i-1}$ have all equal length $b$ [1].

We first address the exact computation of the components of the end to end vector $\boldsymbol{R_e} \equiv \boldsymbol{R}_N - \boldsymbol{R}_0 = \sum_{i=1}^{N} \boldsymbol{r}_i$ of a stretched FJC and the relative variances. At equilibrium, the conformations of the chain are distributed according to the stretching energy $-\boldsymbol{f}\cdot\boldsymbol{R_e}$, where $\boldsymbol{f}$ is the applied external force. The key point of the derivation is that the force is coupled independently to each segment: $-\boldsymbol{f}\cdot\boldsymbol{R_e} = -\sum_i \boldsymbol{f}\cdot\boldsymbol{r_i}$. It is thus possible to calculate the partition function of a single segment, that is $q(\beta f b) = \int d\boldsymbol{r} \exp(\beta \boldsymbol{f}\cdot\boldsymbol{r_i})\delta\left(|\boldsymbol{r_i}| - b\right) = 4\pi b^2 \sinh(\beta f b)/\beta f b$ and then compute the partition function of the whole chain $Q$ as $Q = q^N$. Starting from $Q(\beta f b)$ and choosing a reference frame with the $z$ axis oriented along the force, a straightforward computation leads to the well-known result [1] $\langle \boldsymbol{R_e}\rangle = Nb\,\mathcal{L}\,\mathbf{e_z}$, where $\gamma \equiv \beta f b$ and $\mathcal{L} \equiv \coth(\gamma) - 1/\gamma$ is the Langevin function. Analogously, the variances of the three components of $\boldsymbol{R_e}$ are $\sigma_x^2 = \sigma_y^2 = Nb^2 g$ and $\sigma_z^2 = Nb^2 a$, where $g \equiv \mathcal{L}/\gamma$ and $a \equiv 1 - 2g - \mathcal{L}^2$. Collecting these results, we obtain the mean value of the square of the end to end distance:

$$\left\langle \boldsymbol{R_e}^2 \right\rangle = Nb^2(1-\mathcal{L}^2) + N^2 b^2 \mathcal{L}^2 \ , \tag{1}$$

and of the radius of gyration (see section S1)

$$\left\langle R_g^2 \right\rangle = \frac{1}{6} N b^2 + \frac{1}{12} N^2 b^2 \mathcal{L}^2 \, . \tag{2}$$

As expected, we find the unperturbed results $\left\langle \boldsymbol{R_e}^2 \right\rangle \simeq Nb^2, \left\langle R_g^2 \right\rangle \simeq Nb^2/6$ when $\gamma \to 0$, and the typical values of a rod $\left\langle \boldsymbol{R_e}^2 \right\rangle \simeq N^2 b^2, \left\langle R_g^2 \right\rangle \simeq N^2 b^2/12$ in the limit of infinite forces. The transition between the two regimes takes place at a force $\gamma_c \sim 1/\sqrt{N}$, in agreement with previous perturbative results [21].

The radius of gyration is a useful quantity to measure the spatial extent of a macromolecule. Nevertheless, it cannot capture the presence of anisotropies, which ultimately determine the overall shape of the polymer. In this respect, a more suitable tool is the inertia tensor $\mathcal{T}$, whose elements are $\mathcal{T}_{\alpha\beta} = \frac{1}{N+1}\sum_{i=0}^{N}(\alpha_i - \alpha_{cm})(\beta_i - \beta_{cm})$, where $\alpha, \beta \in \{x, y, z\}$ and $\boldsymbol{R}_{cm} \equiv (x_{cm}, y_{cm}, z_{cm})$ is the position of the center of mass of the chain [22]. The eigenvalues $\lambda_1 \geq \lambda_2 \geq \lambda_3 \geq 0$ of $\mathcal{T}$ are proportional to the square of the semiaxes of the ellipsoid which best approximates the shape of the polymer, while the corresponding eigenvectors describe its orientation. Moreover, by construction $R_g^2 = \lambda_1 + \lambda_2 + \lambda_3$. Strikingly, when it comes to shape properties even the simplest models for polymers give non-trivial results. As already noticed in an early work by Kuhn [23], in spite of the spherical symmetry of the system, the typical shape of an unperturbed FJC is an elongated ellipsoid, whose random orientation preserves the overall symmetry. Numerical computations have shown that the ensemble averages of the eigenvalues of an unperturbed FJC are in the ratios $\langle\lambda_1\rangle : \langle\lambda_2\rangle : \langle\lambda_3\rangle = 11.8 : 2.7 : 1$, thus outlining a pronounced asymmetry in the spatial distribution of the monomers [22].

In order to characterize the shape of a stretched chain, we evaluated the eigenvalues of the inertia tensor and the corresponding eigenvectors by means of Monte Carlo simulations (for details see section S2 in the Supplemental Material). In Fig.1 we show a schematic picture recapitulating the evolution of the polymer as the tension is increased. As the picture qualitatively shows, the effect of an external force on a chain is twofold. For low values of $\gamma$, the tension mostly affects the orientation of the enveloping ellipsoid, aligning it along its direction [24] (left region in Fig.1). Correspondingly, in Fig.2 and in Fig.S1 in the Supplemental Material we show the average value of $\cos\psi_s$,

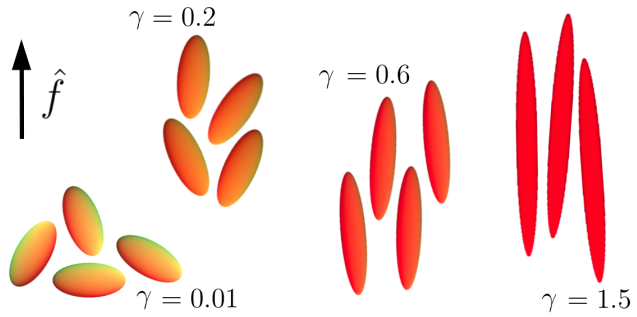


FIG. 1. Schematic illustration of the effect of an external force on a FJC. The arrow indicates the direction of the external force. All the ellipsoids shown have axes ratios corresponding to the average values of the eigenvalues for a chain made of $N = 200$ segments and for the values of $\gamma$ reported in the figure. Particularly, we show the projection corresponding to the two largest eigenvalues. To ease visualization, the absolute size of the ellipsoids was chosen arbitrarily, thus relative sizes of ellipsoids drawn for different values of $\gamma$ do not reflect the real values.

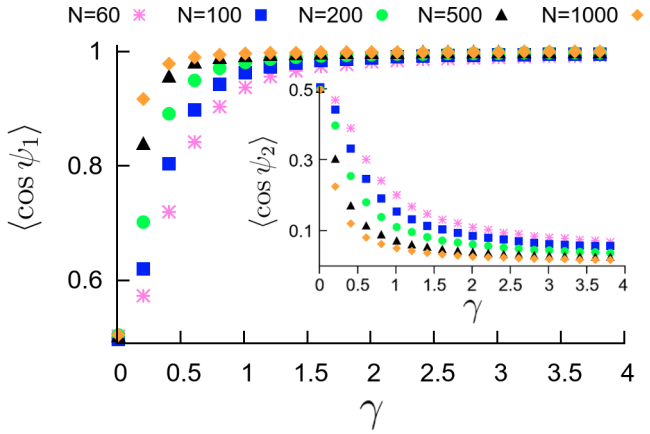


FIG. 2. Orientation of the ellipsoid enveloping a stretched FJC as a function of the adimensionalized force $\gamma$. In the plot we report for several values of $N$ the average cosine of the angles $\psi_1$ and $\psi_2$ (inset) between the external force and the eigenvectors corresponding to $\lambda_1, \lambda_2$ respectively.

where $\psi_s$ is the angle between the applied force and the eigenvector corresponding to the eigenvalue $\lambda_s$. Starting from the typical value of random orientations (1/2), the cosine rapidly approaches 1 in the case of $\lambda_1$ (Fig.2) and 0 for $\lambda_2$ (Fig.2 inset) and $\lambda_3$ (Fig.S1), which correspond to an ellipsoid with the principal axis oriented along the force. It is worth noting that the cosine approaches its large-$\gamma$ value more rapidly for larger sizes of the chain. After this "dipole-like" regime, the tension strongly deforms the polymer, thus leading to an increase in the anisotropy of its shape (right region in Fig.1). However, we note that, due to the monotonicity of $\mathcal{L}^2$, $R_g^2$ increases monotonically from its unperturbed value to the rodlike limit, thus a weak streching is present also at low forces. After the ellipsoid has aligned to the force, $\lambda_1$ gives the largest contribution to $R_g^2$. From Eq.(2), we thus expect $\langle \lambda_1 \rangle \simeq N^2 b^2 L^2/12$, which is verified by MC simulations (Fig.3 top), with small but systematic deviations that decrease for longer chains. For large forces, the two remaining eigenvalues are expected to behave as the transverse contributions to $R_g^2$, and are governed by the fluctuations of the chain on the plane perpendicular to the force. Comparing the formula for $\sigma_{x,y}$, we thus predict that in this regime $\langle \lambda_2 \rangle \simeq c_2 N b^2 g$ and $\langle \lambda_3 \rangle \simeq c_3 N b^2 g$, where $c_2$ and $c_3$ are numeric constants. This ansatz is confirmed in Fig.3 center, where the continuos curves are obtained by tuning the coefficients in order to globally fit the MC data obtained for $\gamma > 1$ and correspond to $c_2 = 0.100 \pm 0.001$ and $c_3 = 0.034 \pm 0.001$. Intriguingly, $\langle \lambda_2 \rangle$ and $\langle \lambda_3 \rangle$ show a non-monotonic behavior for small forces. More in detail, starting from $\gamma = 0$ they increase up to a maximum, after which they decrease according to the large-$\gamma$ behavior. A comparison with the corresponding values of $\langle \cos \psi_2 \rangle, \langle \cos \psi_3 \rangle$ (Fig.2 and Fig.S1) shows that the range of forces with increasing $\lambda_2, \lambda_3$ corresponds to a regime where the ellipsoid has still to align with the force. Therefore, an intuitive explanation of this phenomenon is that, due to the random orientation of the polymer (see left region in Fig.1), on average in this regime the force deforms the ellipsoid almost isotropically, thus leading to an increase of all the eigenvalues. In contrast, after a perfect alignment has been achieved (right region in Fig.1), only $\langle \lambda_1 \rangle$ keeps growing, while the two smaller eigenvalues shrink

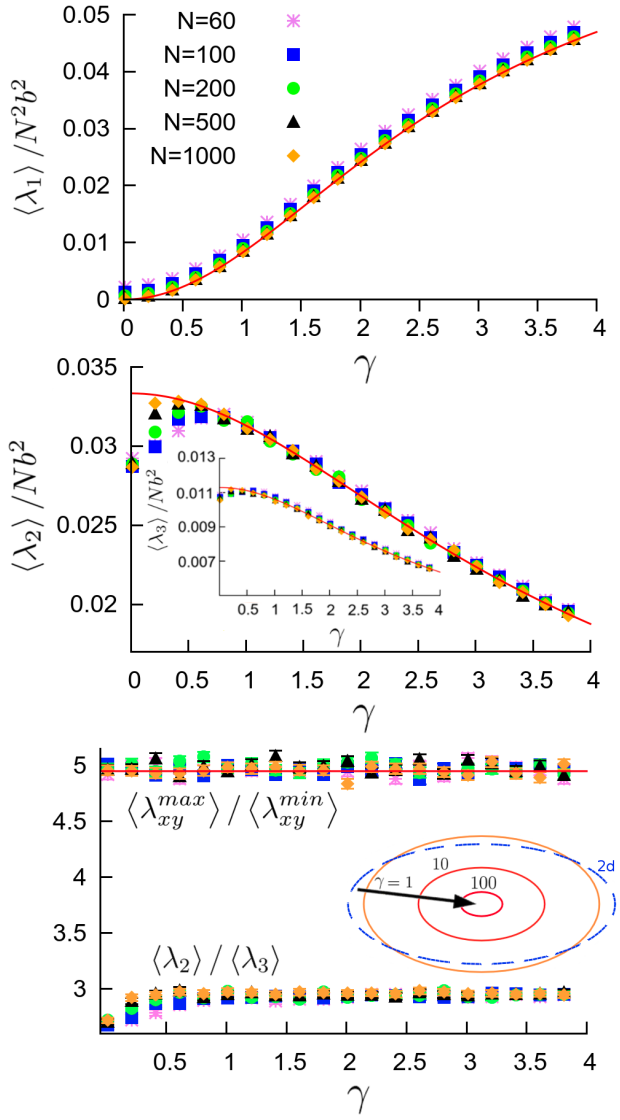


FIG. 3. Top and center panels: normalized eigenvalues $\lambda_1/N^2b^2$ (top), $\lambda_2/Nb^2$ (center) and $\lambda_3/Nb^2$ (center inset) as a function of the adimensionalized force $\gamma$, for several values of chain size $N$. The continuous curves are the corresponding fitting functions reported in the main text. Bottom panel: aspect ratio of the $xy$ projection of the chain and of the transverse section of the ellipsoid. The continuous red line shows the aspect ratio of a pure two-dimensional FJC, which we computed by means of MC simulations and found to be equal to $4.95 \pm 0.01$. Inset: sketch of the shape of the transverse section of the chain for $\gamma = 1, 10, 100$, where the axes are proportional to $\sqrt{\lambda_2}$ and $\sqrt{\lambda_3}$ (continuous lines). The arrow indicates the direction of increasing $\gamma$. The blue dashed line sketches the typical shape of a two-dimensional FJC.

due to the smaller and smaller fluctuations in the directions perpendicular to the force. Notably, in the large-force regime $\langle\lambda_2\rangle / \langle\lambda_3\rangle = c_2/c_3 \simeq 3$ for all values of $N$ (Fig.3 bottom), implying that the section of the ellipsoid shrinks while preserving a universal shape independent of the size of the polymer (inset). Since for $\gamma \gg 1$ the chain is almost aligned with the external force, one would expect to identify the universal section of the ellipsoid with the projection of the chain onto the $xy$ plane that, because of the independence of the three directions of a Random Walk, has the same features of a two-dimensional FJC. The shape properties of the $xy$ projection of the chain are obtained by diagonalizing the submatrix of the inertia tensor identified by the elements $\mathcal{T}_{xx}, \mathcal{T}_{xy}, \mathcal{T}_{yy}$. As we report in Fig.3 bottom, the ratio between the averages of its eigenvalues $\lambda_{xy}^{max}$ and $\lambda_{xy}^{min}$ closely follows the behavior of a two-dimensional FJC (red continuous curve), but is larger than $\langle\lambda_2\rangle / \langle\lambda_3\rangle$. Why do the transverse section and the $xy$ projection of the ellipsoid have different shapes? Qualitatively, the key point is that, although the main axis of the ellipsoid becomes more and more aligned with the external force, the value of $\lambda_1$ increases with $\gamma$, therefore its projection onto the $xy$ plane is comparable to the contributions coming from $\lambda_2$ and $\lambda_3$. From a quantitative point of view, we note that

the total contribution to $\langle R_g^2 \rangle$ involving the $x$ and $y$ coordinates is equal to $Nb^2g/3 \simeq 0.33Nb^2g$ (see section S1). Nevertheless, the large-force formulas provided above for $\langle \lambda_2 \rangle, \langle \lambda_3 \rangle$ show that the sum of the smaller eigenvalues is $\langle \lambda_2 \rangle + \langle \lambda_3 \rangle = (c_2 + c_3)Nb^2g \simeq 0.13Nb^2g$. Therefore, also $\langle \lambda_1 \rangle$ is expected to give a significant contribution to the $x, y$ projection of the FJC equal to $c_1 Nb^2 g$, where $c_1 = 1/3 - c_2 - c_3 \simeq 0.20$ (as we show in section S3, the same result can be found starting directly from the MC data for $\langle \lambda_1 \rangle$). These results show that the isotropically-shrinking transverse section of the ellipsoid cannot be identified with the $xy$ projection of the FJC, thus outlining a novel universal behavior in the shape of polymers.

By analyzing the behaviour of the eigenvalues of the inertia tensor, we have characterized the increasing anisotropy of a stretched chain. A useful global index to quantify this anisotropy is provided by the asphericity [22, 25]

$$\mathcal{A} \equiv \frac{\sum_s \left\langle \left(\lambda_s - \bar{\lambda}\right)^2 \right\rangle}{6 \left\langle \bar{\lambda}^2 \right\rangle} = \frac{3 \left\langle \mathrm{Tr}\, \left(\mathcal{T}^2\right) \right\rangle}{2 \left\langle \left(\mathrm{Tr}\, \mathcal{T}\right)^2 \right\rangle} - \frac{1}{2}\,, \tag{3}$$

where $\bar{\lambda} = \sum_s \lambda_s/3$ is the arithmetic mean of the eigenvalues. For a perfectly-symmetric distribution, all the eigenvalues have equal magnitude $\lambda_s = \bar{\lambda}$, so that $\mathcal{A} = 0$. In the opposite limit of a rod-like chain, one eigenvalue dominates over the others ($\lambda_1 \gg \lambda_2, \lambda_3$) and as a result $\mathcal{A} = 1$. The asphericity of an unperturbed FJC can be computed analytically, and it has been shown that, at the leading term, $\mathcal{A} = 10/19 \simeq 0.53$, independently of $N$ [22]. According to Eq. (3), in order to compute $\mathcal{A}$ we need to calculate the averages $\left\langle \mathrm{Tr}\, \left(\mathcal{T}^2\right) \right\rangle$ and $\left\langle \left(\mathrm{Tr}\, \mathcal{T}\right)^2 \right\rangle$, which can be written explicitly as a combination of quadratic terms of $\mathcal{T}$ (see section S4). Such terms can always be decomposed as sums of end-to-end distances of independent subportions of the chain, whose average can be computed by means of our results for $\langle \boldsymbol{R}_e^2 \rangle$ derived above. Proceeding in this way, we could compute analytically the asphericity of a stretched FJC and find

$$\mathcal{A} = 1 - \frac{72ag + 36g^2 + 24Ng\mathcal{L}^2}{36a^2 + 80ag + 112g^2 + 4\mathcal{L}^2(11a + 10g)N + 5N^2\mathcal{L}^4} \tag{4}$$

which is shown in Fig.4 as a function of $\gamma$ for different values of $N$ and is in perfect agreement with the average values of asphericity from MC simulations. The limiting behaviors of Eq. (4) are very instructive. For $N\mathcal{L}^2 \gg 1$, the contributions involving the size of the polymer dominate the asphericity, and $\mathcal{A} \simeq 1 - 24/5N\gamma\mathcal{L}$. A Taylor expansion around $\gamma = 0$ gives instead $\mathcal{A} \simeq 10/19 + 25N\gamma^2/1083$. Since at low forces $N\gamma\mathcal{L} \sim N\gamma^2$, we can conclude that the asphericity depends on $N$ and $\gamma$ by means of the combination $N\gamma\mathcal{L}$ in both the limiting cases, which suggests this to be the case, at the leading order, in the whole range of forces. As we show in the inset of Fig.4, the data nicely collapse onto the same curve if $\mathcal{A}$ is plotted as a function of $N\gamma\mathcal{L}$.

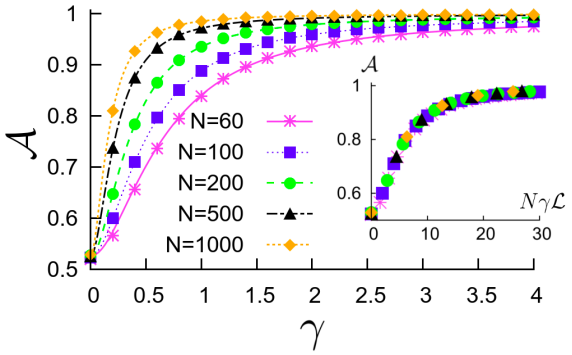


FIG. 4. Comparison between Monte Carlo data and exact formula (Eq. (4)) for the aspericity $\mathcal{A}$ as a function of the adimensionalized force $\gamma$, for several values of $N$. If the data are plotted as a function of $N\gamma\mathcal{L}$, all the sets approximately collapse onto a universal curve (inset).

Also the orientation of the ellipsoid depends, to the leading order, on the same combination of chain length and force: the average cosines $\langle \cos \psi_s \rangle$ (compare Fig.2 and Fig. S1) collapse onto a universal curve when plotted as a function of $N\gamma\mathcal{L}$ (Fig.5). The alignment of the ellipsoid to the external force is analogous to the behavior of an electric dipole in the presence of an external field [26], although here a 180° rotation results in the same physical state. In this case the dipole moment is epitomized by the elongation of the chain, and thus we can interpret the factor $N\mathcal{L}$ as being proportional to the polarization response of the dipole: larger values of $N$ result into a more responsive chain,

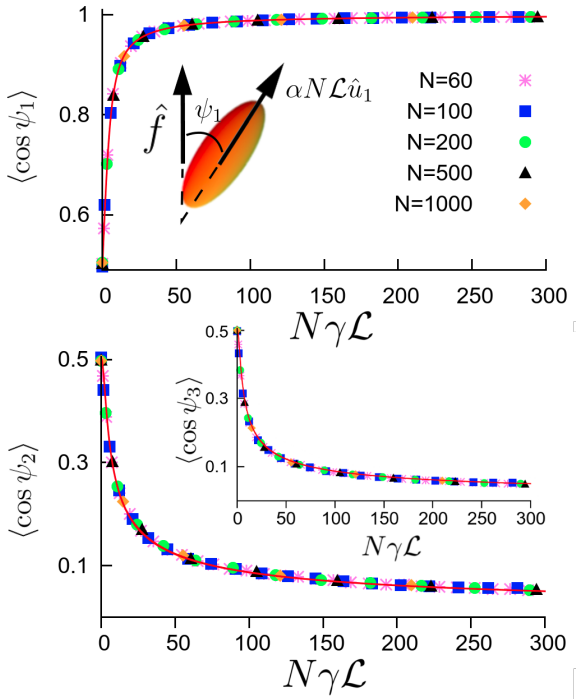


FIG. 5. Top panel: collapse of the average value of $\cos\psi_1$ (compare Fig.2) when plotted as a function of $N\gamma\mathcal{L}$. In the inset we show a schematic picture of the dipole analogy. Bottom panel: collapse of $\langle\cos\psi_2\rangle$ and $\langle\cos\psi_3\rangle$. The three continuous curves are the predictions obtained from the electric-dipole analogy.

although at large forces the dipole moment saturates to an asymptotic value. In other words, we assume the dipole to have a moment equal to $\alpha N\mathcal{L}$, where $\alpha$ is a proportionality constant, and to be directed along the main axis of the ellipsoid, as sketched in Fig.5. Within this assumption, the interaction energy is equal to $\alpha N\gamma\mathcal{L}\cos\psi_1$, and the average cosines are equal to (see section S5)

$$\langle\cos\psi_1\rangle = \frac{1}{1-e^{-\alpha N\gamma\mathcal{L}}} - \frac{1}{\alpha N\gamma\mathcal{L}} \tag{5}$$

and

$$\langle\cos\psi_2\rangle = \langle\cos\psi_3\rangle = \frac{I_1(\alpha N\gamma\mathcal{L})}{\sinh(\alpha N\gamma\mathcal{L})}\,, \tag{6}$$

where $I_1$ is the modified Bessel function of the first kind.

The constant $\alpha$ can be determined by considering the large-force behavior. Indeed, from Eq. (5) we can estimate the average sinus of $\psi_1$ for $\gamma \gg 1$ as $\langle\sin\psi_1\rangle \simeq \sqrt{1-\langle\cos\psi_1\rangle^2} \simeq \sqrt{2/\alpha N\gamma\mathcal{L}}$. Moreover, remembering that $\lambda_1$ is proportional to the square of the best-fitting ellipsoid and that its $xy$ projection is given by $c_1 Nb^2 g$, by construction we also have $\langle\sin\psi_1\rangle = \sqrt{c_1 Nb^2 g/\langle\lambda_1\rangle} \simeq \sqrt{12c_1 Nb^2 g/N^2b^2\mathcal{L}^2} = \sqrt{12c_1/N\gamma\mathcal{L}}$. As a result, we thus find that $\alpha = 1/6c_1 \simeq 0.83$ which, by means of Eqs. (5) and (6), leads to the continuous curves showed in Fig.5. The remarkable agreement between our ansatz and the simulations shows that the dipole analogue can capture even quantitatively the behavior of the ellipsoid in the whole range of forces.

In conclusion, starting from the exact distribution of the end-to-end vector, in this work we have characterized in detail the properties of a stretched FJC. Our results show that both the shape ($\langle\lambda_s\rangle, \mathcal{A}$) and the orientation ($\langle\cos\psi_s\rangle$) of the polymer are dominated by finite-size effects. In the case of infinite $N$, any non-zero value of the force would result in a rod-like chain aligned with the external force, in line with the linear-response "entropic spring" result, according to which for small $\gamma$ the relative elongation of the polymer along the direction of the force follows a Hooke-like formula $\boldsymbol{f} = 3k_BT\boldsymbol{R_e}/Nb^2$ [1], which in the limit of infinite chain length corresponds to an infinitely soft polymer. Here, we have also quantitatively addressed the corrections introduced by finite values of $N$, showing that at the leading order both shape and orientation depend on $N$ and $\gamma$ only through their combination $N\gamma\mathcal{L}$ and providing analytical formulas for them. Moreover, we have shown that the transverse section of the ellipsoid shrinks

isotropically according to novel universal shape features. Though derived for a FJC, our results for small forces can be directly applied to a wide variety of models, such as *e.g.* the Wormlike Chain in the case of double-stranded DNA [27], provided that the contour length of the chain is much larger than its Kuhn length [1] but still short enough so that excluded-volume effects can be neglected [28].

The authors thank the Swiss National Science Foundation for support under the grants 513469 (P.D.L.R. and A.S.S.) and 200021-138073 (P.D.L.R. and S.A.).

[1] M. Rubinstein and R. H. Colby, *Polymer Physics* (Oxford University Press, Oxford, 2003).
[2] A. P. Minton, Biophys. J. **78**, 101 (2000).
[3] R. I. Dima and D. Thirumalai, J. Phys. Chem. B **108**, 6564 (2004).
[4] C. E. Cordeiro, M. Molisana, and D. Thirumalai, J. Phys. II France **7**, 433 (1997).
[5] D. J. Bonthuis, C. Meyer, D. Stein, and C. Dekker, Phys. Rev. Lett. **101**, 108303 (2008).
[6] C. Micheletti and E. Orlandini, Macromolecules **45**, 2113 (2012).
[7] G. Zifferer and W. Preusser, Macromol. Theory Simul. **10**, 397 (2001).
[8] K. Alim and E. Frey, Phys. Rev. Lett. **99**, 198102 (2007).
[9] E. J. Rawdon, J. C. Kern, M. Piatek, P. Plunkett, A. Stasiak, and K. C. Millett, Macromolecules **41**, 8281 (2008).
[10] W. K. Lim and A. R. Denton, J. Chem. Phys. **141**, 114909 (2014).
[11] M. S. Cheung, D. Klimov, and D. Thirumalai, Proc. Nat. Academ. Sci. **102**, 4753 (2005).
[12] D. Homouz, M. Perham, A. S. M. S. Cheung, and P. Wittung-Stafshede, Proc. Nat. Academ. Sci. **105**, 11754 (2008).
[13] C. Bustamante, Z. Bryant, and S. B. Smith, Nature **421**, 423 (2003).
[14] K. E. Matlack, B. Misselwitz, K. Plath, and T. A. Rapoport, Cell **97**, 553 (1999).
[15] W. Neupert and M. Brunner, Nat. Rev. Mol. Cell. Biol. **3**, 555 (2002).
[16] L. Liu, R. T. McNeilage, L. X. Shi, and S. M. Theg, Plant Cell **113**, 1246 (2014).
[17] B. Liu, Y. Han, and S. Qian, Mol. Cell **49**, 453 (2013).
[18] D. H. Goldman, C. M. Kaiser, A. Milin, M. Righini, I. T. Jr., and C. Bustamante, Science **348**, 457 (2015).
[19] S. Assenza, P. De Los Rios, and A. Barducci, Front. Mol. Biosci. **2**, 8 (2015).
[20] F. Ritort, J. Phys.: Condens. Matter **18**, R531 (2006).
[21] R. M. Neumann, Biophys. J. **2**, 34183420 (2002).
[22] J. Rudnick and G. Gaspari, J. Phys. A: Math. Gen. **19**, L191 (1986).
[23] W. Kuhn, Kolloid-Zeitschrift **68**, 2 (1934).
[24] C. Micheletti, D. Marenduzzo, and E. Orlandini, Physics Reports **504**, 1 (2011).
[25] J. Rudnick and G. Gaspari, *Elements of the Random Walk* (Cambridge University Press, Cambridge, 2004).
[26] R. M. Neumann, Phys. Rev. A **31**, 3516(R) (1985).
[27] J. F. Marko and E. D. Siggia, Macromolecules **28**, 8759 (1995).
[28] T. Strick, J.-F. Allemand, V. Croquette, and D. Bensimon, Progr. Biophys. Mol. Biol. **74**, 115 (2000).

# Supplemental Material for

# The Shape of a Stretched Polymer

Alberto S. Sassi, Salvatore Assenza & Paolo De Los Rios

## S1 - EXACT COMPUTATION OF $\langle \boldsymbol{R_g^2} \rangle$

In the present section, we evaluate the mean squared radius of gyration, extending a method that has been used, for example by Rubinstein and Colby [1], for the calculation of $\langle R_g^2 \rangle$ of an unperturbed Freely-Jointed Chain.

The radius of gyration can be written as

$$\langle R_g^2 \rangle = \left\langle \frac{1}{2(N+1)^2} \sum_{i,j} (\mathbf{R}_i - \mathbf{R}_j)^2 \right\rangle = \frac{1}{(N+1)^2} \sum_{j>i} \langle (\mathbf{R}_i - \mathbf{R}_j)^2 \rangle \ . \tag{7}$$

The term inside the two brackets is the end to end vector of the subchain delimited by monomer in position $i$ and $j$. Implementing the exact formula for $\langle \boldsymbol{R_e^2} \rangle$ reported in the main text, we easily find

$$\langle R_g^2 \rangle = \frac{1}{(N+1)^2} \sum_{i=0}^{N} \sum_{j=i}^{N} \left[ (j-i) b^2 \left(1 - \mathcal{L}^2\right) + (j-i)^2 b^2 \mathcal{L}^2 \right] \simeq \frac{1}{6} N b^2 + \frac{1}{12} N^2 b^2 \mathcal{L}^2 \,, \tag{8}$$

where we have neglected all the terms which are sublinear in $N$.

The contribution involving only the $x$ and $y$ coordinates can be explicitly computed in a similar fashion. Denoting the position vector of the $i$-th monomer as $\mathbf{R}_i \equiv (X_i, Y_i, Z_i)$

$$\frac{1}{(N+1)^2} \sum_{j>i} \left\langle (X_j - X_i)^2 \right\rangle + \left\langle (Y_j - Y_i)^2 \right\rangle = \frac{2}{(N+1)^2} \sum_{j>i} \left\langle (X_j - X_i)^2 \right\rangle \,, \tag{9}$$

where we substituted $\left\langle (Y_j - Y_i)^2 \right\rangle = \left\langle (X_j - X_i)^2 \right\rangle$ because of the cylindrical symmetry of the system. By means of the exact distribution of the end-to-end vector reported in the main text, we finally find

$$\frac{2}{(N+1)^2} \sum_{j>i} \left\langle (X_j - X_i)^2 \right\rangle = \frac{2}{(N+1)^2} \sum_{i=0}^{N} \sum_{j=i}^{N} (j-i) b^2 g \simeq \frac{1}{3} N b^2 g \,. \tag{10}$$

The contribution involving the $z$ coordinate can be computed by following the same strategy, yielding as a final result

$$\frac{1}{(N+1)^2} \sum_{j>i} \left\langle (Z_j - Z_i)^2 \right\rangle \simeq \frac{1}{6} N b^2 a + \frac{1}{6} N b^2 \mathcal{L}^2 + \frac{1}{12} N^2 b^2 \mathcal{L}^2 = \frac{1}{6} N b^2 (1 - 2g) + \frac{1}{12} N^2 b^2 \mathcal{L}^2 \,. \tag{11}$$

Naturally, summing Eq. (10) and Eq. (11) one retrieves the formula for the radius of gyration reported in Eq. (8).

## S2 - DETAILS OF THE MONTE CARLO SIMULATIONS

The main features of the shape of a stretched FJC were investigated by means of both analytical computations and MC simulations. The latter were performed extracting the orientation of each tangent vector directly from the distribution $p(\boldsymbol{r})$, which we report here for convenience:

$$p(\boldsymbol{r}) = \frac{\beta f b}{4\pi b^2 \sinh(\beta f b)} \exp(\beta \boldsymbol{f} \cdot \boldsymbol{r}) \delta\left(|\boldsymbol{r}| - b\right) . \tag{12}$$

More in detail, thanks to the cylindric symmetry of the problem, the azimuthal angle $\varphi$ could be simply extracted uniformly in the range $[0, 2\pi]$. As for the polar angle $\vartheta$, a little workaround was needed in order to map its distribution onto uniform sampling. Let $x$ be a random number uniformly distributed in the range $[0, 1]$. By construction, the infinitesimal probability to find a number in the interval $[x, x + dx]$ is simply given by $dx$. As for the angle $\vartheta$, by considering only the polar contribution to equation (12) and remembering that $\gamma \equiv \beta f b$, we easily find for the distribution of its cosine

$$\tilde{p}(\cos\vartheta) = \frac{\gamma}{2\sinh\gamma} e^{\gamma\cos\vartheta} . \tag{13}$$

Since the mapping has to preserve the infinitesimal probability of corresponding values of $\theta$ and $x$, the following condition has to be satisfied:

$$\tilde{p}(\cos\vartheta) d\cos\vartheta = dx . \tag{14}$$

Integrating both sides, we thus get

$$\frac{1}{2\sinh\gamma}\left[e^{\gamma\cos\vartheta} - e^{\gamma}\right] = x , \tag{15}$$

where the integration constant was fixed by imposing $\theta(x = 0) = 0$. Therefore, for each step the polar angle $\vartheta$ was computed by inverting

$$\cos\vartheta = \frac{\log(e^{\gamma} - 2x\sinh\gamma)}{\gamma} . \tag{16}$$

For each value of $N$ and $\gamma$, the mean values of the several quantities considered in the main text are obtained by averaging $10^4$ different realizations. Statistical error is estimated by normalizing the standard deviation of the results and, when not shown, is always smaller than the size of symbols in the figures.

## S3 - ANALYSIS OF SUBLEADING TERMS IN $\lambda_1$

In the present section we focus on the various terms contributing to $\lambda_1$ in the large-force regime. In section S1 we computed the contributions to the radius of gyration coming from the $xy$ projection (Eq. (10)) and the $z$ component (Eq. (11)) of the FJC. For $\gamma \gg 1$, $\lambda_1$ is expected to give the leading contribution to the $z$ component as well as to play a significant role in quantitatively determining the $xy$ projection. Therefore, we predict the following functional form:

$$\langle\lambda_1\rangle = \frac{1}{6}Nb^2(1 - 2g) + \frac{1}{12}N^2b^2\mathcal{L}^2 + c_1 Nb^2 g . \tag{17}$$

Starting from the MC data reported in Fig. 3 top in the main text, we thus considered the combination

$$\lambda_1^{\text{sub}} \equiv \langle\lambda_1\rangle - \frac{1}{6}Nb^2(1 - 2g) - \frac{1}{12}N^2b^2\mathcal{L}^2 . \tag{18}$$

According to Eq. (17), the following formula should thus hold

$$\frac{\lambda_1^{\text{sub}}}{Nb^2} = c_1 g . \tag{19}$$

As we show in Fig.7, the MC data collapse onto a universal curve when $\lambda_1^{\text{sub}}$ is normalized by the chain size $N$. Moreover, by tuning the numeric constant $c_1$ they are well described by the function $g$, as expected from Eq. (19). The optimum value of the constant is $c_1 = 0.204 \pm 0.001$, in perfect agreement with the result found in the main text starting from the fits of $\lambda_2$ and $\lambda_3$.

## S4 - EXACT COMPUTATION OF ASPHERICITY

In the case of the asphericity the idea is the same as for the radius of gyration, but a larger number of terms must be evaluated. We first rewrite the formula in the following way:

$$\langle A \rangle \;=\; \frac{3\left\langle Tr\left[\mathcal{T}^2\right]\right\rangle}{2\left\langle \left(Tr\left[\mathcal{T}\right]\right)^2\right\rangle} - \frac{1}{2} \;\equiv\; \frac{3\sum_{\alpha=1}^{3}\sum_{\beta=1}^{3}\left\langle \mathcal{T}_{\alpha\beta}\mathcal{T}_{\beta\alpha}\right\rangle}{2\sum_{\alpha=1}^{3}\sum_{\beta=1}^{3}\left\langle \mathcal{T}_{\alpha\alpha}\mathcal{T}_{\beta\beta}\right\rangle} - \frac{1}{2}\;, \tag{20}$$

where we are using Greek letters as labels for spatial coordinates $(x, y, z)$. We have to find the values of two terms, that we write more explicitly:

$$\langle \mathcal{T}_{\alpha\beta}\mathcal{T}_{\beta\alpha}\rangle = \frac{1}{N^4}\sum_{i=0}^{N}\sum_{j=i}^{N}\sum_{k=0}^{N}\sum_{l=k}^{N}\left\langle \left(\alpha_j-\alpha_i\right)\left(\beta_j-\beta_i\right)\left(\alpha_l-\alpha_k\right)\left(\beta_l-\beta_k\right)\right\rangle \;, \tag{21}$$

$$\langle \mathcal{T}_{\alpha\alpha}\mathcal{T}_{\beta\beta}\rangle \;=\; \frac{1}{N^4}\sum_{i=0}^{N}\sum_{j=i}^{N}\sum_{k=0}^{N}\sum_{l=k}^{N}\left\langle \left(\alpha_j-\alpha_i\right)^2\left(\beta_l-\beta_k\right)^2\right\rangle \;. \tag{22}$$

Since the tensor is symmetric, only six terms are independent: $\mathcal{T}^2_{xx}$, $\mathcal{T}^2_{xy}$, $\mathcal{T}^2_{xz}$, $\mathcal{T}^2_{zz}$, $\mathcal{T}_{xx}\mathcal{T}_{yy}$, $\mathcal{T}_{xx}\mathcal{T}_{zz}$. The most complicated are the ones with equal indices, $\mathcal{T}^2_{xx}$ and $\mathcal{T}^2_{zz}$. We will calculate $\mathcal{T}^2_{zz}$. All the other terms can be evaluated in a similar way. We must treat separately three different cases:

$\boxed{I)\;\; i<j<k<l}$

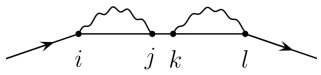


In this case there is no overlap between the intervals $(i, j)$ and $(k, l)$ and the mean of a product becomes the product of means:

$$[I] = \; 2\frac{1}{N^4}\sum_{i=0}^{N}\sum_{j=i}^{N}\sum_{k=j}^{N}\sum_{l=k}^{N}\left\langle \left(z_j-z_i\right)^2\left(z_l-z_k\right)^2\right\rangle = \tag{23}$$

$$= 2\frac{1}{N^4}\sum_{i=0}^{N}\sum_{j=i}^{N}\sum_{k=j}^{N}\sum_{l=k}^{N}\left\langle \left(z_j-z_i\right)^2\right\rangle\left\langle \left(z_l-z_k\right)^2\right\rangle \;= \tag{24}$$

$$= 2\frac{1}{N^4}\sum_{i=0}^{N}\sum_{j=i}^{N}\left[(j-i)b^2a+\mathcal{L}^2(j-i)^2b^2\right]\sum_{k=j}^{N}\sum_{l=k}^{N}\left[(l-k)b^2a+\mathcal{L}^2(l-k)^2b^2\right] \;, \tag{25}$$

where $a = 1-2g-\mathcal{L}^2$ and we have used the result previously obtained for the $z$ component of the end to end vector.

$\boxed{II)\;\; i<k<j<l}$

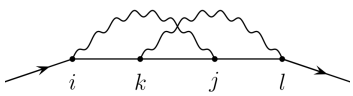

$$[II] \;=\; 2\frac{1}{N^4}\sum_{i=0}^{N}\sum_{k=i}^{N}\sum_{j=k}^{N}\sum_{l=j}^{N}\left\langle (z_j-z_i)^2\,(z_l-z_k)^2\right\rangle \;. \tag{26}$$

Because of the overlap the average cannot be split *directly*. However, this problem can be solved with a trick:

$$\begin{aligned}
&\left\langle (z_j-z_i)^2\,(z_l-z_k)^2\right\rangle \;=\; \left\langle ((z_j-z_k+z_k-z_i)\,(z_l-z_j+z_j-z_k))^2\right\rangle \;=\\
&\left\langle \Big((z_j-z_k)\,(z_l-z_j)+(z_k-z_i)\,(z_l-z_j)+(z_j-z_k)\,(z_k-z_i)+(z_j-z_k)^2\Big)^2\right\rangle \;=\\
&\left\langle (z_j-z_k)^2\,(z_l-z_j)^2\right\rangle+\left\langle (z_k-z_i)^2\,(z_l-z_j)^2\right\rangle+\left\langle (z_j-z_k)^2\,(z_k-z_i)^2\right\rangle+\left\langle (z_j-z_k)^4\right\rangle\\
&+2\left\langle (z_j-z_k)\,(z_k-z_i)\,(z_l-z_j)^2\right\rangle+2\left\langle (z_j-z_k)\,(z_l-z_j)\,(z_k-z_i)^2\right\rangle\\
&+4\left\langle (z_l-z_j)\,(z_k-z_i)\,(z_j-z_k)^2\right\rangle+2\left\langle (z_l-z_j)\,(z_j-z_k)^3\right\rangle+2\left\langle (z_k-z_i)\,(z_j-z_k)^3\right\rangle \;.
\end{aligned}$$

The final expression, even if it is much longer, has a great advantage: now in any product the round brackets are uncorrelated with respect to each other, and we can split the averages:

$$<(\,)\ldots(\,)> \;=\; <(\,)>\;\ldots.\;<(\,)> \;.$$

In this way, each term in the previous equation can be computed as above.

$\boxed{III)\;\; i<k<l<j}$

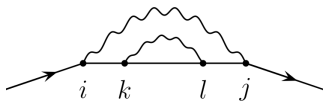


$$[III] \;=\; 2\frac{1}{N^4}\sum_{i=0}^{N}\sum_{k=i}^{N}\sum_{l=k}^{N}\sum_{j=l}^{N} <(z_j-z_i)^2\,(z_l-z_k)^2> \;. \tag{27}$$

Since the calculation is analogous to the previous one, we will just show how it is possible to decorrelate each term:

$$<(z_j-z_i)^2\,(z_l-z_k)^2> \;=\; <((z_j-z_l+z_l-z_k+z_k-z_i)\,(z_l-z_k))^2>\,, \tag{28}$$

and then the usual calculation is made. For evaluating the mean values we need the following expressions:

$$\begin{aligned}
&{\sigma^2}_z = Nb^2(1-2g-\mathcal{L}^2)\\
&\mu_z = Nb\mathcal{L}\\
&{\sigma^2}_{x,y} = Nb^2 g\\
&\mu_{x,y} = 0\\
&\langle\alpha\rangle \;= \mu_\alpha\\
&\left\langle\alpha^2\right\rangle \;= \mu_\alpha^2+\sigma_\alpha^2\\
&\left\langle\alpha^3\right\rangle \;= \mu_\alpha^3+3\mu_\alpha\sigma_\alpha^2\\
&\left\langle\alpha^4\right\rangle \;= \mu_\alpha^4+3\sigma_\alpha^4+6\mu_\alpha^2\sigma_\alpha^2 \;.
\end{aligned} \tag{29}$$

where $\alpha$ indicates a space coordinate. Keeping only the leading terms, the result is

$$\left\langle \mathcal{T}_{zz}^2\right\rangle \;=\; [I] \;+\; [II] \;+\; [III] \;=\; \frac{N^2b^4}{720}\left(5\mathcal{L}^4N^2+44\mathcal{L}^2Na+36a^2\right)\,, \tag{30}$$

The six moments are

$$\begin{aligned}
\langle \mathcal{T}_{xx}^2 \rangle &= \frac{g^2 N^2 b^4}{20} \\
\langle \mathcal{T}_{xy}^2 \rangle &= \frac{g^2 N^2 b^4}{90} \\
\langle \mathcal{T}_{xx} \mathcal{T}_{yy} \rangle &= \frac{g^2 N^2 b^4}{36} \\
\langle \mathcal{T}_{zz}^2 \rangle &= \frac{N^2 b^4}{720} \left(5\mathcal{L}^4 N^2 + 44\mathcal{L}^2 N a + 36a^2\right) \\
\langle \mathcal{T}_{xz}^2 \rangle &= \frac{g N^2 b^4}{360} \left(4a + 3\mathcal{L}^2 N\right) \\
\langle \mathcal{T}_{xx} \mathcal{T}_{zz} \rangle &= \frac{g N^2 b^4}{72} \left(2a + \mathcal{L}^2 N\right) \ .
\end{aligned} \tag{31}$$

Substituting in equation (S4), we finally find the mean asphericity

$$\langle A \rangle = 1 - \frac{72ag + 36g^2 + 24Ng\mathcal{L}^2}{36a^2 + 80ag + 112g^2 + 4\mathcal{L}^2 (11a + 10g) N + 5N^2\mathcal{L}^4} \ . \tag{32}$$

which is the formula reported in the main text.

## S5 - COMPUTATION OF ELLIPSOID ORIENTATION WITHIN THE DIPOLE ANALOGY

As explained in the main text, we captured the orientational behavior of the enveloping ellipsoid of a stretched FJC by exploiting the strong resemblance of this system to an electric dipole in the presence of an external field. Starting from the interaction energy $\alpha N \gamma \mathcal{L} \cos\psi_1$, the average cosine of the main axis of the ellipsoid can be straightforwardly computed:

$$\langle \cos\psi_1 \rangle = \frac{\int_0^{\pi/2} \sin\psi_1 \cos\psi_1 e^{\alpha N \gamma \mathcal{L} \cos\psi_1} d\psi_1}{\int_0^{\pi/2} \sin\psi_1 e^{\alpha N \gamma \mathcal{L} \cos\psi_1} d\psi_1} = \frac{1}{1 - e^{-\alpha N \gamma \mathcal{L}}} - \frac{1}{\alpha N \gamma \mathcal{L}} \, , \tag{33}$$

which is Eq. (4) in the main text. We note that the upper bound of the integrals in the previous formula is $\pi/2$ because of the symmetry of the system with respect to a rotation by $\pi$.

In contrast, the computation of $\langle \cos\psi_2 \rangle$ (which, due to the cylindrical symmetry of the dipole analogy is equal to $\langle \cos\psi_3 \rangle$) is more cumbersome, and we report its explicit derivation in what follows. The following formulas will be needed for our computation:

$$\int_0^{2\pi} (\sin\theta)^k \, d\theta = \begin{cases} 0 & \text{if } k \text{ odd} \\ 2\pi \frac{(k-1)!!}{k!!} & \text{if } k \text{ even} \end{cases} \, , \tag{34}$$

$$\int_0^{\pi/2} (\sin\psi)^{2k+1} \, d\psi = \frac{(2k)!!}{(2k+1)!!} \, , \tag{35}$$

$$I_1(x) = \sum_{k=0}^{\infty} \frac{1}{k!(k+1)!} \left(\frac{x}{2}\right)^{2k+1} \, , \tag{36}$$

$$\sinh x = \sum_{k=0}^{\infty} \frac{x^{2k+1}}{(2k+1)!} \, , \tag{37}$$

where in Eqs. (34) and (35) it is intended that the double factorials are equal to 1 for $k = 0$, and in Eq. (36) $I_1(x)$ is the modified Bessel function of the first kind. For a given value of $\psi_2$, one has to consider for the eigenvector $\hat{u}_1$ corresponding to $\lambda_1$ all the possible orientations lying on the plane perpendicular to the versor $\hat{u}_2$ identified by $\psi_2$.

According to the relative orientation of $\hat{u}_1$ and the external force, each specific orientation results into a different interaction energy, *i.e.* a different Boltzmann weight. Quantitatively, let us consider a reference frame where the $z$ axis is oriented along the external force and the $x$ axis is complanar to both $\hat{z}$ and $\hat{u}_2$. In this reference frame, one has $\hat{u}_2 \equiv (\sin\psi_2, 0, \cos\psi_2)$. From here, it is easy to show that a unitary vector lying on the plane perpendicular to $\hat{u}_2$ can be written as $(-\cos\psi_2 \sin\theta, \cos\theta, \sin\psi_2 \sin\theta)$, where $\theta \in [0, 2\pi]$. Therefore, the orientation of $u_1$ with respect to the force is given by $\cos\psi_1 = \sin\psi_2 \sin\theta$, and the corresponding adimensionalized interaction energy between the dipole and the external field is $\alpha N\gamma\mathcal{L}\cos\psi_1 = \alpha N\gamma\mathcal{L}\sin\psi_2\sin\theta$. The total Boltzmann weight corresponding to the given choice of $\psi_2$ is obtained by integrating the Boltzmann weights relative to this energy over all the possible values of $\theta$. Thus

$$\langle\cos\psi_2\rangle = \frac{\int_0^{\pi/2}\sin\psi_2\cos\psi_2\left(\int_0^{2\pi} e^{\alpha N\gamma\mathcal{L}\sin\psi_2\sin\theta}d\theta\right)d\psi_2}{\int_0^{\pi/2}\sin\psi_2\left(\int_0^{2\pi} e^{\alpha N\gamma\mathcal{L}\sin\psi_2\sin\theta}d\theta\right)d\psi_2}\,. \tag{38}$$

We first address the computation of the Boltzmann weight. By Taylor-expanding the exponential, we have

$$\int_0^{2\pi} e^{\alpha N\gamma\mathcal{L}\sin\psi_2\sin\theta}d\theta = \sum_{k=0}^{\infty}\frac{(\alpha N\gamma\mathcal{L}\sin\psi_2)^k}{k!}\int_0^{2\pi}(\sin\theta)^k\,d\theta\,. \tag{39}$$

Making use of Eq.(34) and performing the change of dummy variable $k = 2m$ in the non-vanishing terms of the series, we find

$$\int_0^{2\pi} e^{\alpha N\gamma\mathcal{L}\sin\psi_2\sin\theta}d\theta = 2\pi\sum_{m=0}^{\infty}\frac{(\alpha N\gamma\mathcal{L})^{2m}}{(2m)!}\frac{(2m-1)!!}{(2m)!!}(\sin\psi_2)^{2m}\,. \tag{40}$$

The numerator in Eq.(38) thus becomes

$$\int_0^{\pi/2}\sin\psi_2\cos\psi_2\left(\int_0^{2\pi} e^{\alpha N\gamma\mathcal{L}\sin\psi_2\sin\theta}d\theta\right)d\psi_2 =$$

$$= 2\pi\sum_{m=0}^{\infty}\frac{(\alpha N\gamma\mathcal{L})^{2m}}{(2m)!}\frac{(2m-1)!!}{(2m)!!}\int_0^{\pi/2}\cos\psi_2\,(\sin\psi_2)^{2m+1}\,d\psi_2 =$$

$$= 2\pi\sum_{m=0}^{\infty}(\alpha N\gamma\mathcal{L})^{2m}\,\frac{(2m-1)!!}{(2m)!}\,\frac{(\sin\psi_2)^{2m+2}\Big|_{\psi_2=0}^{\pi/2}}{(2m+2)\,(2m)!!} =$$

$$= 2\pi\sum_{m=0}^{\infty}\frac{(\alpha N\gamma\mathcal{L})^{2m}}{(2m+2)!!\,(2m)!!}\,,$$

where in the last step we exploited the identity $(2m)! = (2m)!!\,(2m-1)!!$. Moreover, since $(2m)!! = 2^m m!$, the previous formula can be rewritten as

$$2\pi\sum_{m=0}^{\infty}\frac{(\alpha N\gamma\mathcal{L})^{2m}}{(2m+2)!!\,(2m)!!} = \frac{2\pi}{\alpha N\gamma\mathcal{L}}\sum_{m=0}^{\infty}\frac{1}{m!\,(m+1)!}\left(\frac{\alpha N\gamma\mathcal{L}}{2}\right)^{2m+1} = 2\pi\frac{I_1(\alpha N\gamma\mathcal{L})}{\alpha N\gamma\mathcal{L}}\,, \tag{41}$$

where we made use of Eq. (36). Analogously, the denominator in Eq. (38) can be explicitely computed as

$$\int_0^{\pi/2}\sin\psi_2\left(\int_0^{2\pi} e^{\alpha N\gamma\mathcal{L}\sin\psi_2\sin\theta}d\theta\right)d\psi_2 =$$

$$= 2\pi\sum_{m=0}^{\infty}\frac{(\alpha N\gamma\mathcal{L})^{2m}}{(2m)!}\frac{(2m-1)!!}{(2m)!!}\int_0^{\pi/2}(\sin\psi_2)^{2m+1}\,d\psi_2 =$$

$$= 2\pi \sum_{m=0}^{\infty} \frac{(\alpha N \gamma \mathcal{L})^{2m}}{(2m)!} \frac{(2m-1)!!}{(2m)!!} \frac{(2m)!!}{(2m+1)!!} =$$

$$= \frac{2\pi}{\alpha N \gamma \mathcal{L}} \sum_{m=0}^{\infty} \frac{(\alpha N \gamma \mathcal{L})^{2m+1}}{(2m+1)!} =$$

$$= 2\pi \frac{\sinh(\alpha N \gamma \mathcal{L})}{\alpha N \gamma \mathcal{L}} , \tag{42}$$

where in the second step we substituted Eq. (35), while in the last step we made use of the Taylor expansion reported in Eq. (37). Substituting Eq.(41) and Eq.(42) into Eq.(38), we finally obtain

$$\langle \cos \psi_2 \rangle = \frac{I_1(\alpha N \gamma \mathcal{L})}{\sinh(\alpha N \gamma \mathcal{L})} , \tag{43}$$

which is the result reported in Eq. (5) in the main text.

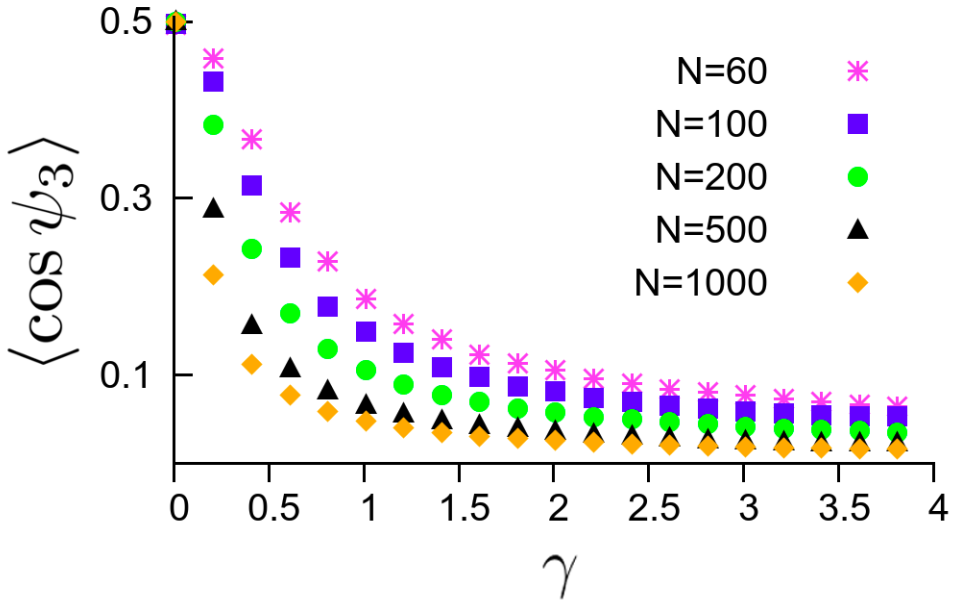


FIG. 6. Average cosine of the angle between the external force and the eigenvector corresponding to $\lambda_3$.

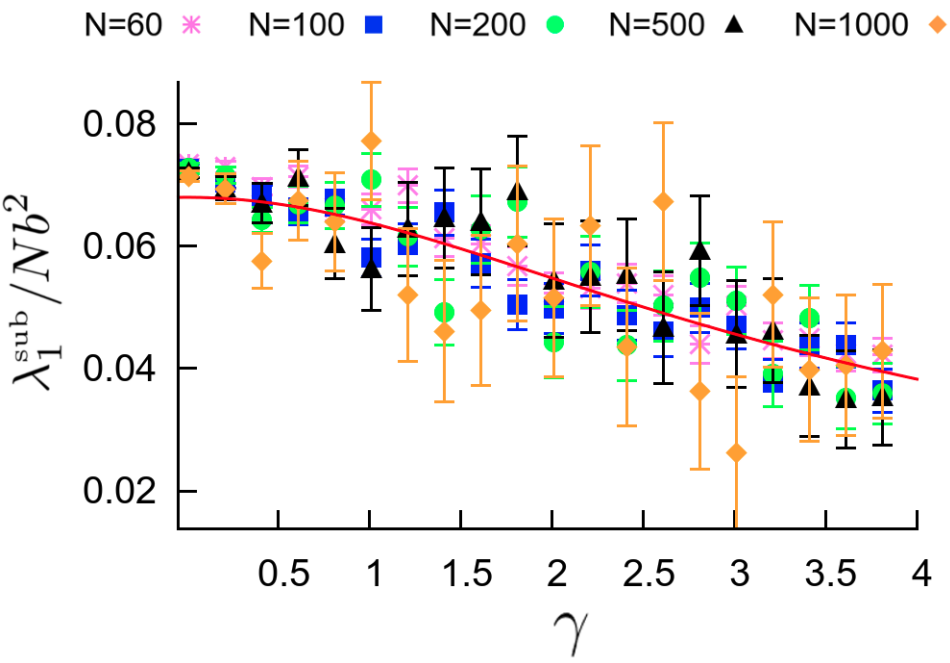


FIG. 7. Plot of $\lambda_1^{\rm sub}/Nb^2$ as a function of $\gamma$ for several values of $N$.